Supplementary Information

Thermally Robust Dy^{3+}-activated $Sc_2Mo_3O_{12}$ Phosphor for Sustainable WLEDs Lighting and Phase Transition-Enabled Visual Cryogenic Thermometry

Annu Balhara,[1,2] Priyansu Mishra,[3] Sreevalsa Subhagan,[4,5] Athira Raghu,[6,7] Ashok Kumar Yadav,[8] Rohit Kumar Gupta,[9] Giri Dhari Patra,[10] V.B. Jayakrishnan,[11] Subrata Das,[4,5] Ashish Kumar Mishra,[9] Santosh K. Gupta[1,2*]

[1]*Radiochemistry Division, Bhabha Atomic Research Centre, Trombay, Mumbai-400085, India*
[2]*Homi Bhabha National Institute, Anushaktinagar, Mumbai-400094, India*
[3]*Mithibai College, Affiliated to University of Mumbai, Mumbai-400056, India*
[4]*Materials Science and Technology Division, CSIR-National Institute for Interdisciplinary Science and Technology, Thiruvananthapuram, Kerala-695019, India*
[5]*Academy of Scientific and Innovative Research (AcSIR), Ghaziabad-201002, India*
[6]*UGC-DAE Consortium for Scientific Research, Mumbai Centre, 246-C Common Facility Building, BARC, Mumbai-400085, India*
[7]*Savitribhai Phule Pune University, Ganeshkhind, Pune-411007, Maharashtra, India*
[8]*Atomic & Molecular Physics Division, Bhabha Atomic Research Centre, Mumbai-400085, India*
[9]*School of Materials Science and Technology, Indian Institute of Technology (BHU), Varanasi-221005, Uttar Pradesh, India*
[10]*Technical Physics Division, Bhabha Atomic Research Centre, Mumbai-400085, India*
[11]*Solid State Physics Division, Bhabha Atomic Research Centre, Mumbai-400085, India*

**To whom correspondence should be addressed. Electronic mail: santoshg@barc.gov.in (SKG)*

S1. Characterization

The powder XRD patterns were acquired on a Proto-AXRD bench top system in the 2θ range of 10-70° using the Cu Kα line (λ = 1.5406 Å) and a scanning rate of 1°/min. Fourier Transform Infrared (FT-IR) spectroscopy was performed in attenuated total reflectance (ATR) mode on a Bruker Alpha II FTIR spectrometer, Germany, in the scanning range from 400 to 4000 cm^{-1} using average of 36 scans. Temperature-dependent Raman studies were performed on a STR-300 micro-Raman spectrometer with an excitation wavelength ~532 nm. The field emission scanning electron microscopy (FE-SEM) was performed on a field emission scanning electron microscope (FE-SEM, Thermofisher) system at a voltage of 20 kV. The X-ray photoelectron spectroscopy measurements were performed on (XPS, Thermo Fisher Scientific) instrument. Rietveld refinement was done on powder XRD patterns by using FullProf software. An X-ray Absorption Spectroscopy (XAS) measurement, which comprises of both X-ray Near Edge Structure (XANES) and Extended X-ray Absorption Fine Structure (EXAFS) techniques, have been carried out on Dy-doped $Sc_2Mo_3O_{12}$ (SMO) at Dy L_3-edge in fluorescence mode. The XAS measurements have been

carried out at the Energy-Scanning EXAFS beamline (BL-9) at the Indus-2 Synchrotron Source (2.5 GeV, 100 mA) at Raja Ramanna Centre for Advanced Technology (RRCAT), Indore, India.[1,2] Photoluminescence studies were performed using a continuous Xenon lamp (450 W) source on a FLS 1000 fluorescence spectrometer (Edinburgh Instruments, U.K.), and visible-PMT as the detector. The temperature-dependent PL studies were performed using the cryostat assembly equipped with FLS-1000 fluorescence spectrometer and Helium gas as the coolant, over the range of 10–500 K. A temperature controller was used with a heating rate of 5 K/min, allowing a stabilization time of 50 s at each temperature before recording the emission spectra, with an accuracy band of ±2 K. The electroluminescence properties were measured using CCD spectrophotometer (Maya 2000 Pro). The prototype WLEDs were fabricated by pasting a mixture of phosphors onto a 280 nm UV LED chip.

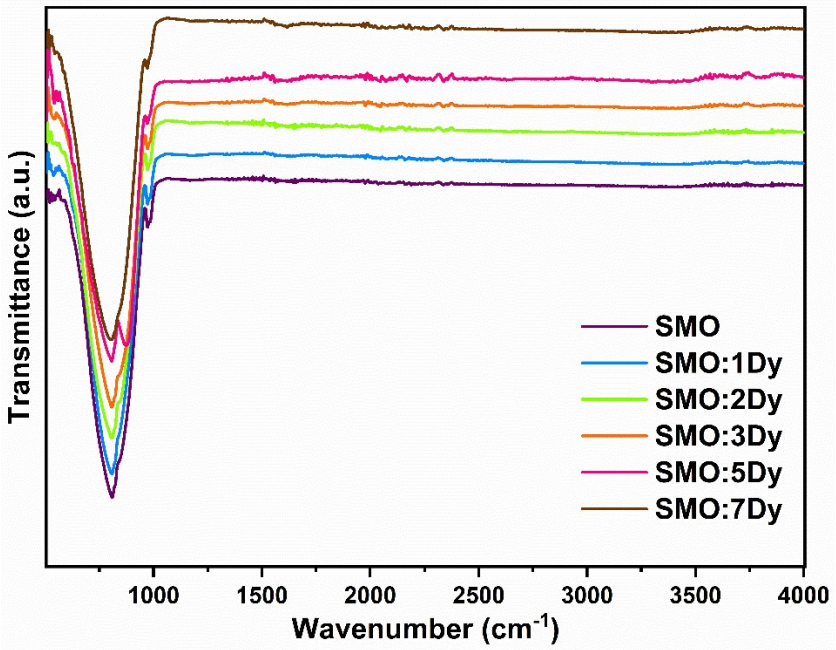

Figure S1: FT-IR of undoped SMO and Dy^{3+}-doped SMO samples.

Table S1: Atom coordinates and crystallographic data of Dy^{3+}-doped SMO obtained after structural refinement.

Atom	x	y	z	B	Occupancy
Sc1	0.11910	0.25080	0.46550	0.455	0.963
Dy	0.11910	0.25080	0.46550	0.455	0.037
Mo1	0.14446	0.10423	0.11747	0.497	1.000
O1	0.07534	0.16280	0.07832	1.710	1.158
O2	0.14489	-0.03086	0.11332	1.420	0.993
O3	0.20080	0.16658	0.01103	1.620	1.204
O4	0.16792	0.12113	0.24511	1.170	1.255
Mo2	0.00000	0.52738	0.25000	0.529	0.500
O5	0.07177	0.45666	0.30425	1.640	1.166
O6	0.04524	0.60576	0.18218	1.710	0.917

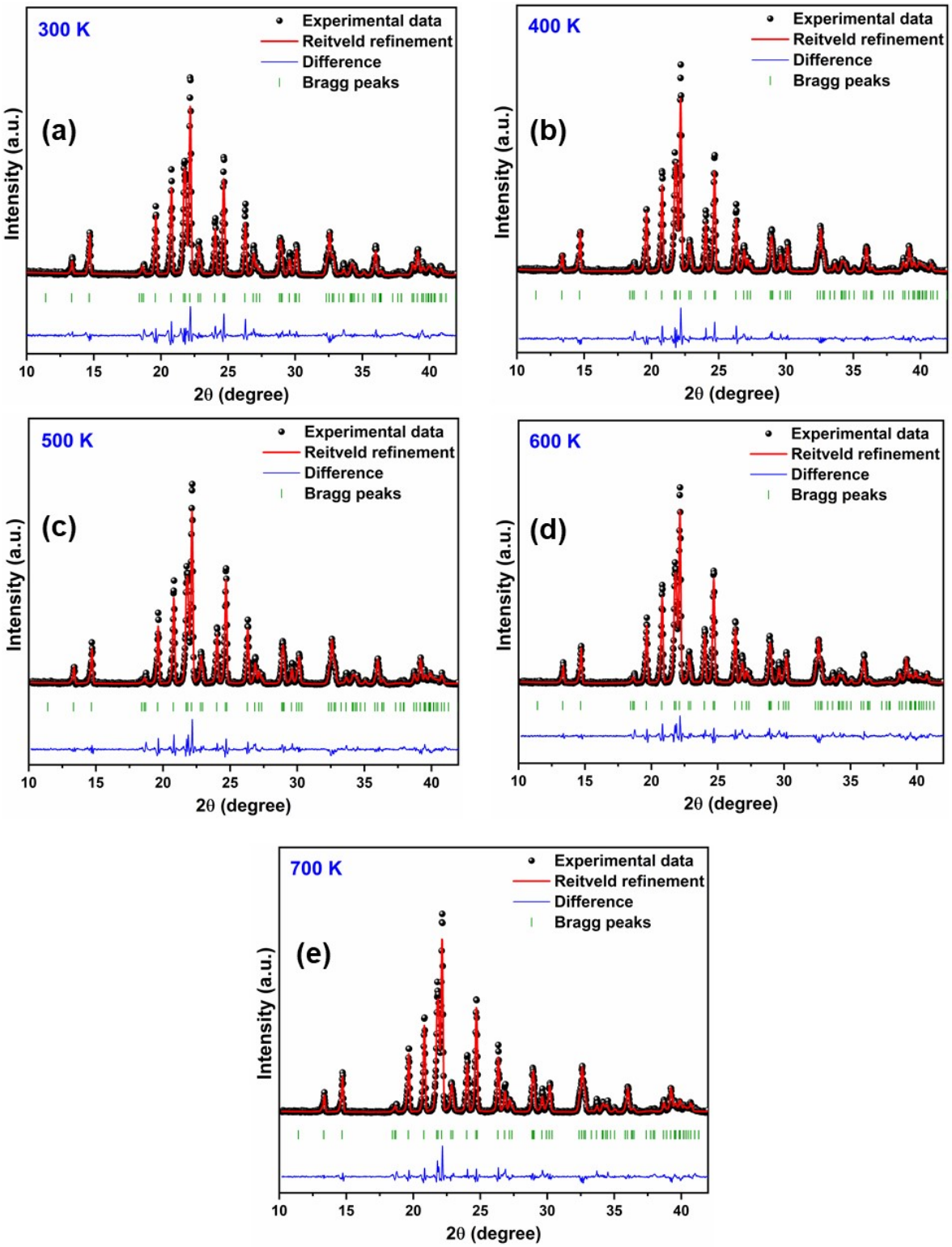

Figure S2: Rietveld refinement of XRD patterns of SMO:3Dy^{3+} sample recorded at different temperatures as (a) 300 K, (b) 400 K, (c) 500 K, (d) 600 K, and (e) 700 K.

Table S2: Lattice parameters obtained on Rietveld refinement of XRD patterns of SMO:3Dy^{3+} sample.

S. No.	Temperature (K)	Lattice parameters	Goodness of fitting
1.	300	a (Å) = 13.2610 b (Å) = 9.5504 c (Å) = 9.6436 V (Å^3) = 1221.341	χ^2 = 2.52 R_p = 16.3 R_{wp} = 21.8
2.	400	a (Å) = 13.2718 b (Å) = 9.5463 c (Å) = 9.6360 V (Å^3) = 1220.852	χ^2 = 1.85 R_p = 14.0 R_{wp} = 18.8
3.	500	a (Å) = 13.2796 b (Å) = 9.5408 c (Å) = 9.6295 V (Å^3) = 1220.035	χ^2 = 1.87 R_p = 13.9 R_{wp} = 18.9
4.	600	a (Å) = 13.2860 b (Å) = 9.5360 c (Å) = 9.6221 V (Å^3) = 1219.078	χ^2 = 1.85 R_p = 13.9 R_{wp} = 18.8
5.	700	a (Å) = 13.2905 b (Å) = 9.5315 c (Å) = 9.6156 V (Å^3) = 1218.099	χ^2 = 1.77 R_p = 13.5 R_{wp} = 18.3

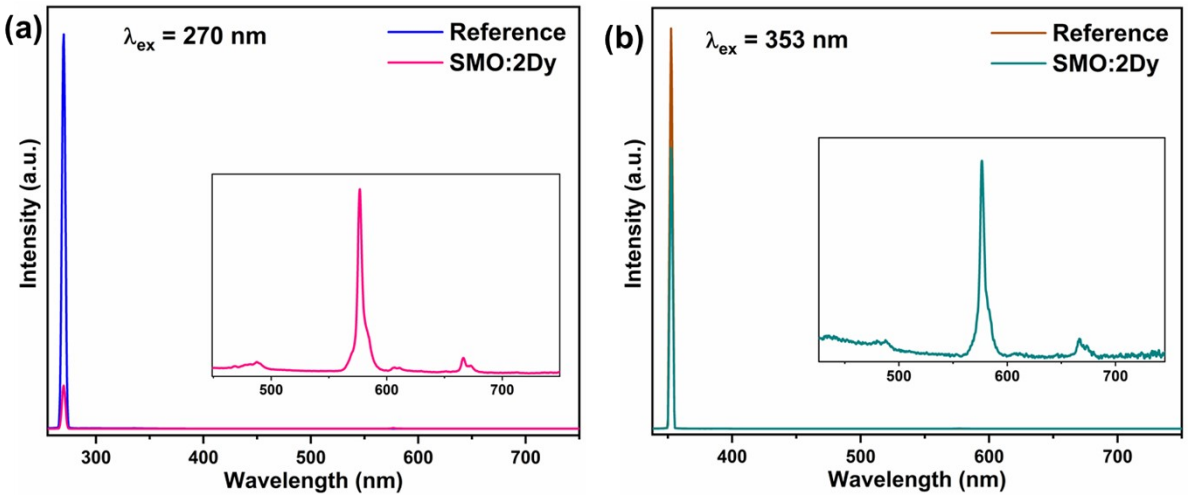

Figure S3: PLQY spectra of SMO:2Dy^{3+} phosphor under (a) CTB (270 nm) and (b) 4*f*→4*f* excitations (353 nm).

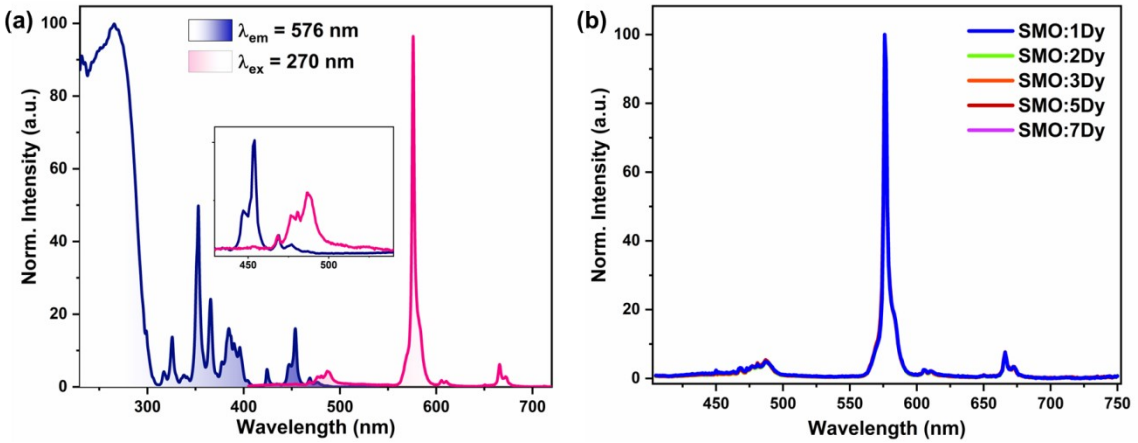

Figure S4: (a) Normalized PLE and emission spectra of SMO:2Dy^{3+} phosphor (inset shows PLE and emission spectra normalized at 468 nm). (b) Normalized emission spectra of doped SMO:*x*Dy^{3+} phosphors with different Dy^{3+} concentrations.

Table S3: Lifetime values of SMO:*x*Dy^{3+} phosphors at 576 nm emission and under 270 nm excitation.

Sample	τ_1 (μs)	%	τ_2 (μs)	%	τ_{avg} (μs)
SMO:1Dy	205.91	19.24	484.91	80.76	431.23
SMO:2Dy	171.74	22.73	436.11	77.27	376.02
SMO:3Dy	164.02	27.56	437.69	72.44	362.27
SMO:4Dy	138.57	34.63	390.00	65.37	302.93
SMO:5Dy	116.94	38.95	358.56	61.05	264.45

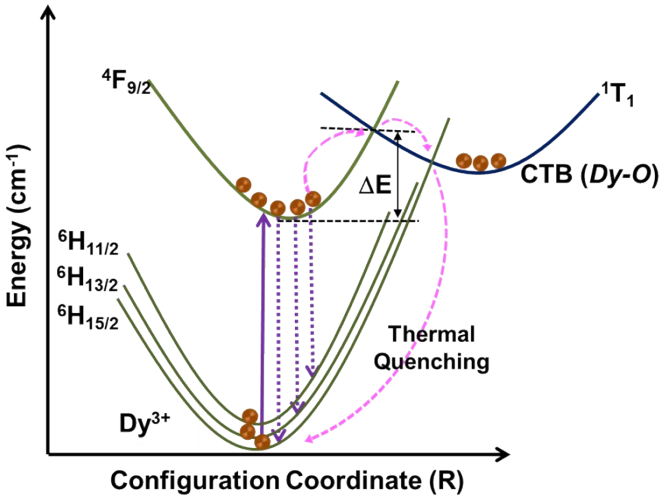

Figure S5: Configurational coordinate diagram showing Dy^{3+} transitions and non-radiative thermal quenching channels.

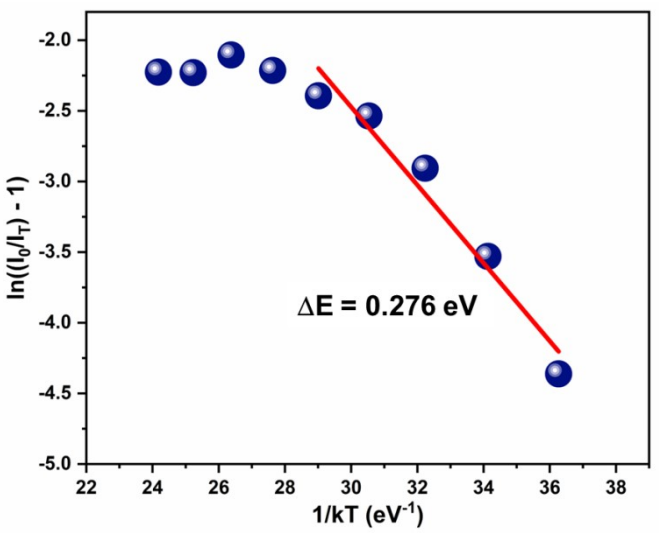

Figure S6: Linear fit of the ln((I$_0$/I)-1) versus 1/kT plot of SMO:2Dy^{3+} phosphor.

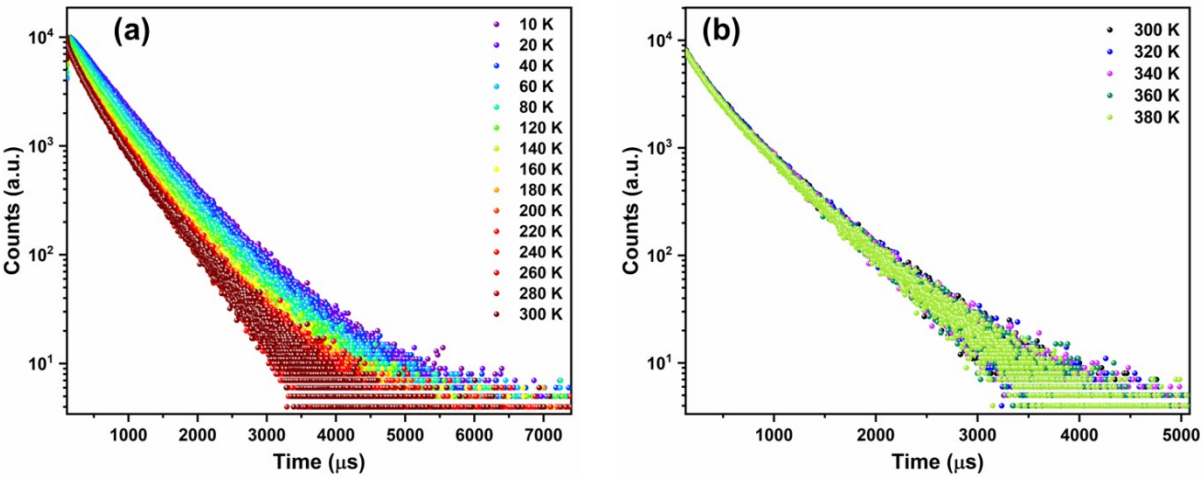

Figure S7: Temperature-dependent decay curves of Dy^{3+} emission at 576 nm within the temperature range of (a) 10 – 300 K and (b) 300 – 380 K.

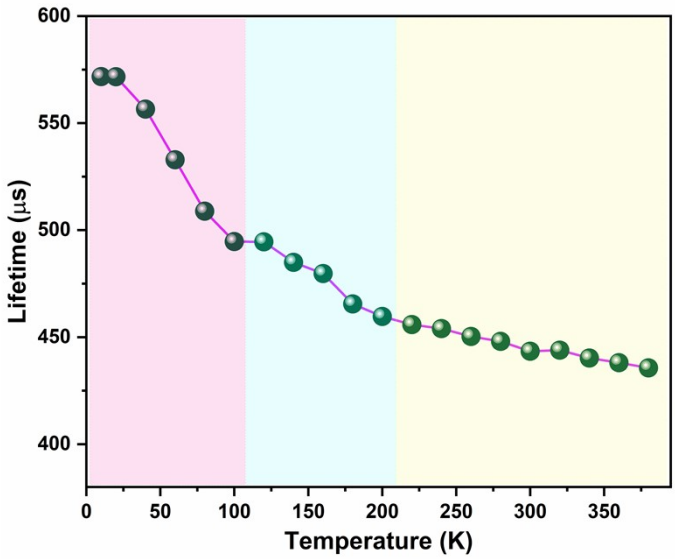

Figure S8: Temperature-dependent lifetime values of SMO:2Dy^{3+} phosphor.

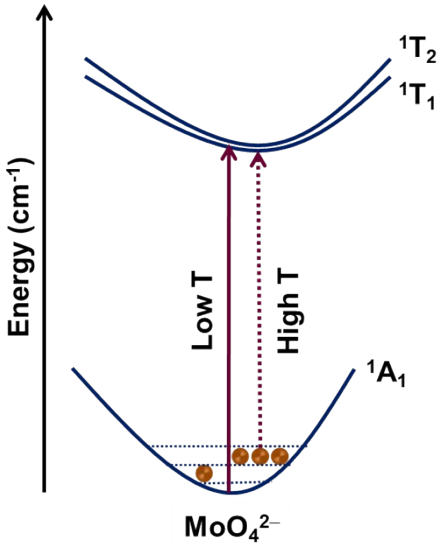

Figure S9: Configurational coordinate diagram showing the thermal population of photoelectrons in the MoO_4^{2-} vibrational sublevels with rise in temperature.

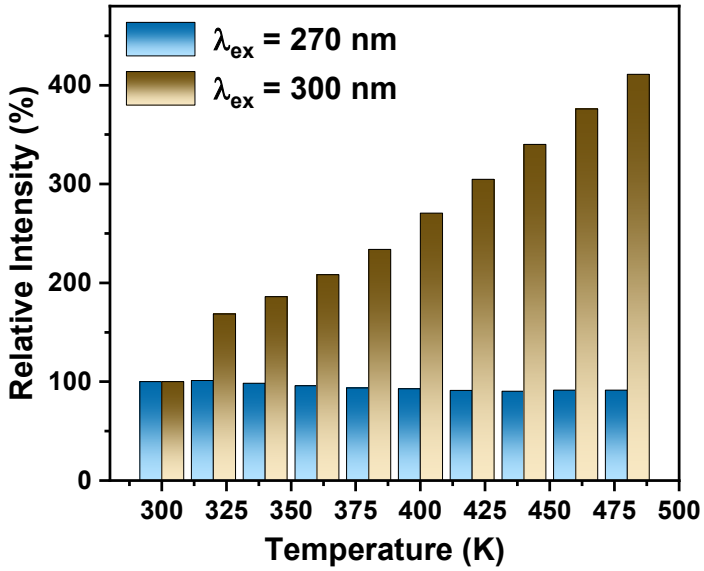

Figure S10: Relative thermal behaviour of Dy^{3+} emission under two different excitation wavelengths i.e., CTB peak (270 nm) and CTB edge (300 nm).

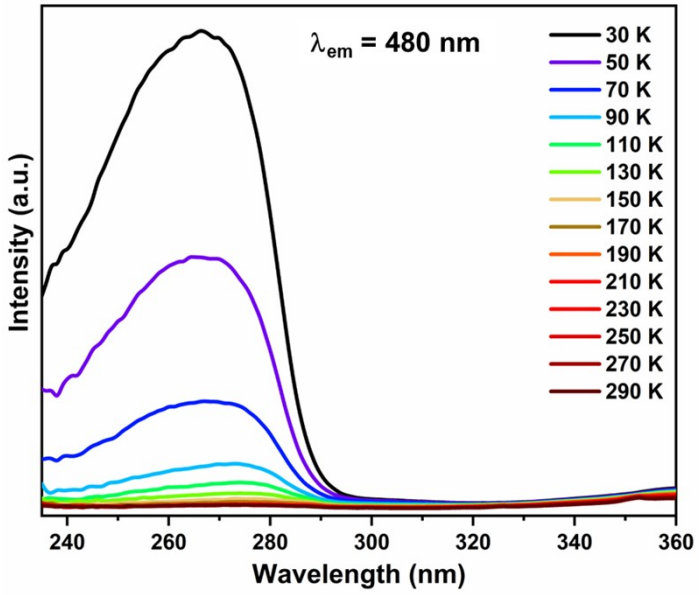

Figure S11: Low temperature-dependent PLE spectra of SMO:2Dy^{3+} monitored at 480 nm.

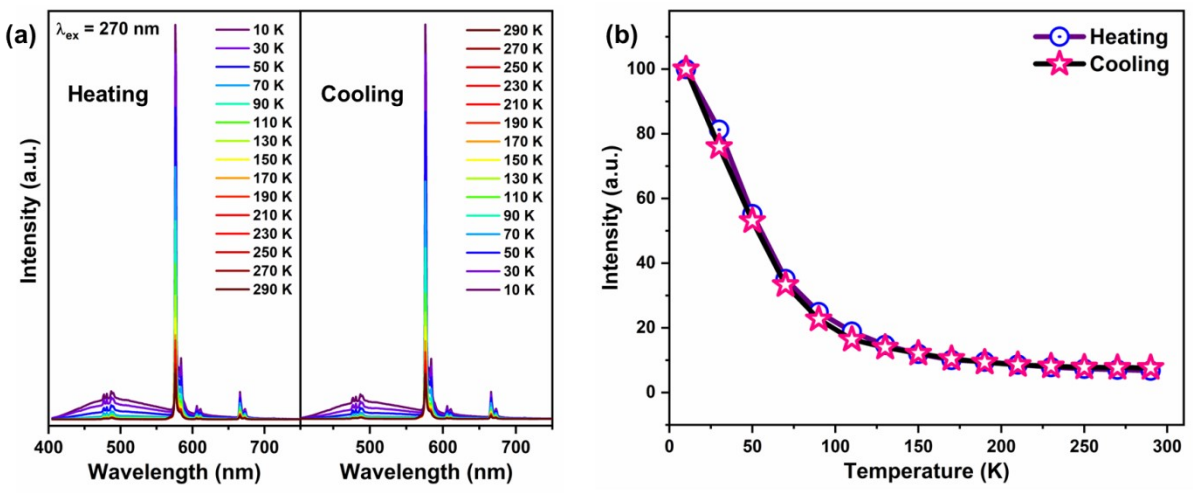

Figure S12: (a) Temperature-dependent emission spectra of SMO:2Dy^{3+} phosphor during the heating and cooling cycles. (b) Reversibility of thermometric luminescence behaviour.

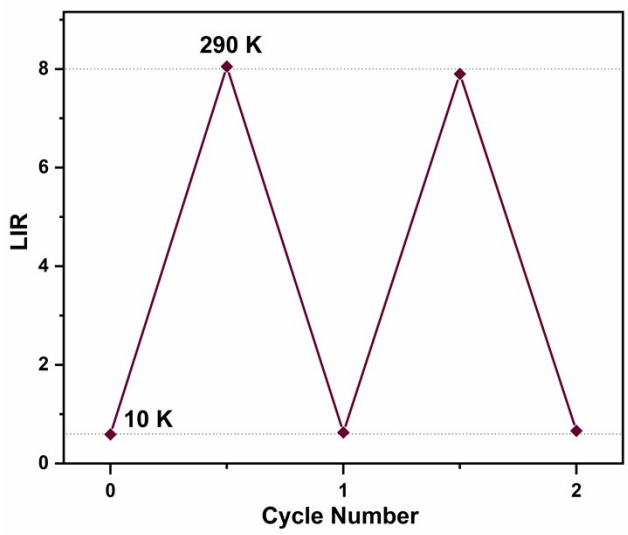

Figure S13: LIR measurements for 2 cycles of heating and cooling.

Table S4: Comparison of SMO:Dy^{3+} phosphor with relevant phosphor materials reported for optical thermal sensing.

System	Type	Temperature Range	Maximum S_r (% K^{-1}) at T (K)	Reference
$GdVO_4:Sm^{3+}$	CTB edge red-shift	300–480 K	3.68% K^{-1} at 300 K	3
$LiTaO_3:Eu^{3+}$	CTB edge red-shift	298 –573 K	1.186% K^{-1} at 423K	4
$K_3LuSi_2O_7:Eu^{3+}$	CTB edge red-shift	298–573 K	1.478% K^{-1} at 323 K	5
$LuVO_4:Eu^{3+}$	CTB edge red-shift	293–573 K	5.023% K^{-1} at 298 K	6
$NaYGeO_4:Eu^{3+}$	CTB edge red-shift	300–570 K	3.60% K^{-1} at 300 K	7
$CaWO_4$:Dy	CTB Intensity	300–650 K	4.66% K^{-1} at 300 K	8
$Gd_{10}V_2O_{20}:Dy^{3+}$	I_{Dy}/I_{V-O}	10–480 K	2.67% K^{-1} at 130 K	9
$Sr_9Ga(PO_4)_7:Dy^{3+}$	I_{Ga-O}/I_{Dy}	298–598 K	0.87% K^{-1} at 598 K	10
$CaWO_4:Tb^{3+}$	CTB shift	303–783 K	1.28% K^{-1} at 303 K	11
$LaVO_4:Eu^{3+}$	CTB-based	98–723 K	1.49% K^{-1} at 303 K	12
$YVO_4:Eu^{3+}$	CTB-based	300–500 K	0.65% K^{-1} at 500 K	13
$Ba_2MgTeO_6:Eu^{3+}$	Absorption edge-based	150–370 K	0.89% K^{-1} at 240 K	14
$Ca_9ZnK(VO_4)_7:Sm^{3+}$	$I(Sm)/I(VO_4^{3-})$	300–475 K	2.059%	15

			K^{-1} at 350 K	
$Na[(Gd_{0.8}Eu_{0.1}Tb_{0.1})SiO_4]$	Ratiometric Thermometer	12–450 K	1.0% K^{-1} at 50 K	**16**
$Li_3Y_3Te_2O_{12}:Dy^{3+}$	Intensity ratios	80–300 K	1.2% K at 80 K	**17**
$Ca_{2.5}Hf_{2.5}Ga_3O_{12}:Dy^{3+}$	thermally coupled energy levels	298–523 K	2.12% K^{-1} at 298 K	**18**
$YAG:Dy^{3+}$	thermally coupled levels	540–1440 K	0.62 % K^{-1} at 500 K	**19**
$YVO_4:Dy^{3+}$	thermally coupled levels	298–673 K	1.8% K^{-1} at 298 K	**20**
$Sc_2Mo_3O_{12}:Dy^{3+}$	$I(MoO_4^{2-})/I(Sm^{3+})$ CTB shift	10–290 K 300–480 K	2.30% K^{-1} at 70 K 1.14% K^{-1} at 300 K	***This work***

References

1 A. K. Poswal, A. Agrawal, A. K. Yadav, C. Nayak, S. Basu, S. R. Kane, C. K. Garg, D. Bhattachryya, S. N. Jha and N. K. Sahoo, Thapar University, Patiala, Punjab, India, 2014, pp. 649–651.

2 S. Basu, C. Nayak, A. K. Yadav, A. Agrawal, A. K. Poswal, D. Bhattacharyya, S. N. Jha and N. K. Sahoo, *J. Phys.: Conf. Ser.*, 2014, **493**, 012032.

3 S. Zhou, C. Duan and S. Han, *Dalton Trans.*, 2018, **47**, 1599–1603.

4 W. Li, J. Song, C. Liu, W. Qiu and N. Guo, *Ceram. Int.*, 2025, **51**, 53672–53680.

5 W. Li, J. Song, W. Qiu, C. Liu, Y. Yuan, Y. Cui and N. Guo, *J. Photochem. Photobiol. A: Chem.*, 2026, **474**, 116990.

6 C. Liu, S. Qu, C. Jia, W. Qiu and N. Guo, *Inorg. Chem.*, 2025, **64**, 25260–25269.

7 Y. Chen, H. Guo, Q. Shi, J. Qiao, C. Cui, P. Huang and L. Wang, *Inorg. Chem.*, 2024, **63**, 16304–16312.

8 Q. Liu, B. Cao, M. Gao, L. Qiu, Y. Weng, Y. He, X. Han and B. Dong, *J. Mater. Chem. C*, 2024, **12**, 12854–12861.

9 S. Bi, Z. Fan and H. J. Seo, *Mater. Res. Bull.*, 2022, **153**, 111898.

10 X. Yang, Q. Li, X. Li and B. Ma, *Opt. Mater.*, 2020, **107**, 110133.

11 L. Li, F. Qin, L. Li, H. Gao and Z. Zhang, *J. Phys. Chem. C*, 2019, **123**, 6176–6181.

12 I. E. Kolesnikov, D. V. Mamonova, M. A. Kurochkin, V. A. Medvedev and E. Yu. Kolesnikov, *Phys. Chem. Chem. Phys.*, 2022, **24**, 27940–27948.
13 Z. Li, Q. Liang, L. He and X. Wu, *Dalton Trans.*, 2025, **54**, 15474–15482.
14 N. J. Suraja, A. Bindhu, S. K. Solaman and S. Ganesanpotti, *J. Mater. Chem. C*, 2025, **13**, 2470–2484.
15 Z. Wang, N. Liu, J. Kong and Y. Wang, *Dalton Trans.*, 2025, **54**, 10673–10682.
16 D. Ananias, F. A. A. Paz, D. S. Yufit, L. D. Carlos and J. Rocha, *J. Am. Chem. Soc.*, 2015, **137**, 3051–3058.
17 A. Bindhu, J. I. Naseemabeevi and S. Ganesanpotti, *J. Sci.: Adv. Mater. Devices*, 2022, **7**, 100444.
18 S. Long, M. Tian, D. Zhang, X. Luo, W. Xu, Y. Tian and S. Xin, *J. Mater. Chem. C*, 2024, **12**, 19536–19544.
19 Q. Yin, Y. Quan, F. Luo, W. Gong, J. Liu, J. Chai, L. Zhang and J. Liu, *App. Mater. Today*, 2025, **46**, 102889.
20 I. E. Kolesnikov, A. A. Kalinichev, M. A. Kurochkin, E. V. Golyeva, A. S. Terentyeva, E. Yu. Kolesnikov and E. Lähderanta, *Sci. Rep.*, 2019, **9**, 2043.